Canadian Science Publishing | Canadian Journal of Civil Engineering

# Does historic construction suffer or benefit from the urban heat island effect in Ghent and global warming across Europe?

| | |
|---|---|
| Journal: | *Canadian Journal of Civil Engineering* |
| Manuscript ID | cjce-2018-0594.R1 |
| Manuscript Type: | Article |
| Date Submitted by the Author: | 07-Dec-2018 |
| Complete List of Authors: | Vandemeulebroucke, Isabeau; Universiteit Gent Faculteit Ingenieurswetenschappen en Architectuur,<br>Calle, Klaas; Universiteit Gent Faculteit Ingenieurswetenschappen en Architectuur<br>Caluwaerts, Steven; Universiteit Gent Vakgroep Vakgroep Fysica en Sterrenkunde<br>De Kock, Tim; Universiteit Gent Vakgroep Geologie en Bodemkunde<br>Van Den Bossche, Nathan; Universiteit Gent Faculteit Ingenieurswetenschappen en Architectuur |
| Keyword: | HAM simulations, solid historical masonry, retrofit, Urban Heat Island, climate change |
| Is the invited manuscript for consideration in a Special Issue? : | Durability and Climate Change |
| | |

# Does historic construction suffer or benefit from the urban heat island effect in Ghent and global warming across Europe?

Isabeau Vandemeulebroucke[1], Klaas Calle[1], Steven Caluwaerts[2], Tim De Kock[3], Nathan Van Den Bossche[1]

**Abstract:** Renovating historical buildings having valuable facades often includes interior retrofitting, perhaps entailing an increased durability risk. However, the urban heat island effect and the ongoing climate change might mitigate the severity of frost action and mould growth. By means of HAM simulations in Delphin, this study evaluates interior retrofitting of solid masonry on three scales. First, the sensitivity to the intra-urban climatic differences of the freeze-thaw in Ghent is analysed. Secondly, the spatial pattern of freeze-thaw behaviour across Europe is assessed. Finally, the influence of observed climate change on the European freeze-thaw pattern is investigated. A decreasing number of critical freeze-thaw-cycles is found when comparing the rural area and city centre of Ghent. Further due to climate change, the number of freeze-thaw-cycles across Europe generally decreases as well, except at northern latitudes exposed to increased wind-driven rain loads.

*Key words*: HAM simulations, solid historical masonry, retrofit, Urban Heat Island, climate change.

(7568 words)



## I. INTRODUCTION

A major part of the building stock in Belgium consists of buildings, either in historical or contemporary, with masonry brick walls. Along with their structural purpose, masonry wall assemblies also act as moisture barriers (Straube et al. 2011). Amongst the variety of wall types, the solid masonry wall assembly has been frequently used in the past and is thereby typically found in many historical buildings. The moisture buffer against wind-driven rain (WDR) is achieved through the thickness of the

[1] Department of Architecture and Urbans Planning, Faculty of Engineering and Architecture, Ghent University, Ghent, Belgium; corresponding author: Isabeau Vandemeulebroucke, Sint Pietersnieuwstraat 41 B4 – 9000 Ghent, Belgium, +32 498 57 30 73, Isabeau.Vandemeulebroucke@UGent.be
[2] Department of Physics and Astronomy, Faculty of Sciences, Ghent University, Ghent, Belgium
[3] Department of Geology, Faculty of Sciences, Ghent University, Ghent, Belgium

masonry, typically having a width of one and a half bricks (Straube and Schumacher 2007). During WDR events, moisture penetrates the mortar and brick stone and is stored in the pore matrix until conditions are favourable for moisture dissipation, either to the outdoor or indoor climate. Interior insulation retrofits, however, form a thermal and moisture barrier, reducing the masonry's temperature and increase the absorbed moisture content (MC), possibly increasing the risk of moisture related damage (Straube et al. 2011).

An important damage mechanism in masonry is related to the action of freezing and thawing under certain moisture conditions, which causes scaling of the surface and finally leads to disintegration of the material (Wardeh and Perrin 2008; Lisø et al. 2007). Damage is induced by consecutive freeze-thaw-cycles ($FTC_{crit}$) combined with the exceedance of a critical degree of moisture saturation ($S_{crit}$) as introduced by Fagerlund (1973). More severe damage is observed when the $S_{crit}$ is reached. Straube et al.'s (2010) pilot study indicates that the $S_{crit}$ varies significantly between different types of historical brick: 87%, 25% and 30% respectively in modern extruded clay brick, historical brick obtained from the Upper Canada College, and historical brick collected in Old Montreal. These values have been determined by means of non-destructive laboratory testing, using frost dilatometry. For not frost resistant masonry materials, the critical $S_{crit}$ is considered to be 30% according to the WTA Merkblatt 6-5 (2014). Furthermore, a certain MC in porous media remains unfrozen at temperatures below 0°C. Especially in small pores, the freezing point depression leads to the presence of supercooled liquid water. For this reason $FTC_{crit}$ are likely to occur at temperatures well below 0°C depending on the material (Walder and Hallet 1985; Wessman 1997; Straube and Schumacher 2006; Zhou et al. 2017). For granite and marble, relatively compact stone materials, Walder and Hallet (1985) found that the crack growth due to sustained freezing is most efficient between -4°C and -15°C. Straube and Schumacher (2006) suggest that no significant damage in masonry occurs during FTC reaching temperatures between 0°C and -5°C. Zhou et al. (2017) as well propose to consider the freezing point depression when analysing the freeze-thaw risk of building materials.

Beside frost action, also mould growth can induce deterioration of building materials. However, due to the inorganic nature of brick stone, this study only considers mould growth as a threat to the indoor air quality and occupant's health (WHO 2009; Sedlbauer 2001; Viitanen and Ojanen 2007). The four major conditions that initiate mould growth are moisture, temperature, exposure time and substrate (Viitanen and Ritschkoff 1991; Hukka and Viitanen 1999; Viitanen and Ojanen 2007). Minor influencing factors are oxygen concentration, alkalinity, UV radiation, spore availability, air flow, salt concentration in the substrate etc. (Aden 1994).

Nowadays, many historical buildings demand for repurposing, as the requirements of society have changed over the past century. Renovation often involves retrofitting, as legislation has become severe with regards to energy use and efficiency. Although exterior insulation is the better retrofitting choice, this is often not allowed because of the historical and esthetical value of the façade. Interior insulation is sometimes an alternative, despite the increased durability risks. However, the urban heat island (UHI) effect (Oke 1979) might mitigate the frost action in urbanized environments. Next to that, the Intergovernmental Panel on Climate Change assessed that there is clear observational evidence of anthropogenic influence on

the climate during the previous decades (IPCC 2013). The ongoing and future climate change will also impact the durability risks. Therefore, one should consider UHI effects and climate change while assessing the potential decrease in the durability risk of solid masonry wall assemblies.

The UHI in the urban canopy layer (UCL), the air layer below the roof level, is the result of changes in the energy and radiation balance between locations in different urban environments (Oke 1982; Arnfield 2003). In general, the UHI is most pronounced during nights with clear sky conditions and low wind velocity. The UHI can be understood as an interplay between different physical mechanisms (Steward and Oke 2012). The three-dimensional geometry of the buildings in so-called street canyons results in an increased absorption of incoming solar radiation and a greater retention of outgoing infrared radiation. Together with the thermal properties of the materials in an urban environment and the decreased moisture content in the soil, reducing the solar energy converted into latent heat, this explains the elevated air temperature in the UCL. Although it is generally considered as a smaller factor, the anthropogenic release of heat by domestic heating, transport… also contributes to the UHI as investigated for example by Bohnenstengel (2014) for London. Given the spatial variation of the previous contributions significant intra-urban climatic differences exist.

With regards to global warming, Grossi et al. (2007) studied the freeze-thaw risk on the built heritage across Europe using future climate projections obtained from the Hadley HadCM3 global climate model. This study investigates the emission scenario A2 which assumes the largest greenhouse gas emissions among the three scenario's: B1 (low), A1B (mid) and A2 (high). Projections for Europe indicate a temperature increase of 3°C to 5°C. Although, several frost indices are studied by Grossi et al. (2007), the number of FTC crossing 0°C (using daily average temperature) is found a reliable and straightforward approach to evaluate the distribution and change of frost action across the continent. Even a limited temperature increase alters the freeze-thaw behaviour of the climate, shifting the region sustaining the most FTC. An increased number of FTC is expected in regions experiencing an increase in sub-zero mean temperatures, whereas regions experiencing an increase in temperatures above 0°C would sustain less FTC. This means that the number of FTC is decreasing in West and Central Europe, i.e. the temperate climate zone. High latitude regions are likely to experience an increasing number of FTC, along with locations at high altitudes. However, Grossi et al. (2007) does not involve the wall assembly, orientation, WDR load, solar radiation etc. Considering the durability of the built heritage, it is therefore necessary to evaluate these outcomes with the results of HAM simulations on wall assemblies.

The content of this article is the following: The simulation model, boundary conditions, wall construction and damage criteria are discussed in section 2. In section 3, the determination of the critical orientation to assess the durability of the building envelope is elaborated, whereas section 4 analyses the influence of interior retrofitting on solid masonry. Both sections discuss the freeze-thaw behaviour in Ghent and Europe. Additionally, mould growth is considered for the city of Ghent. Beside providing a preliminary context, analysing the critical wall orientation and assembly enables the possibility to focus on the worst-case scenario and delimit the computational cost of the simulations. Section 5, the main objective of this study, analyses

the freeze-thaw behaviour of interior retrofitted solid masonry wall assemblies on three scales. First, the resolution of the city is assessed by considering four locations across the urban environment of Ghent. The influence of UHI effect and other phenomena driving intra-urban differences are evaluated. Secondly, patterns of freeze-thaw behaviour across the European continent are determined. The number of $FTC_{crit}$ is assessed for one statistical average year at 36 locations, and general trends are acknowledged. Finally, a temporal resolution is considered to analyse the influence of observed climate change across Europe at the same 36 locations. Conclusions are formulated in section 6.

## II. Simulation model and criteria

Hygrothermal behaviour and durability of solid masonry wall assemblies are evaluated by means of HAM simulations in Delphin 5.9.5. The Delphin solver has been successfully validated in the past through HAMSTAD Benchmark exercises 1-5 (Nicolai and Grunewald 2006). Further, Matlab Research R2017b is used for the analysis of weather data, the preparation of climatic files and post-processing of simulation results.

HAM simulations are executed for five consecutive years. During the first four years the wall assembly is conditioned to the outdoor climate to achieve a moisture and heat balance, whereas the fifth year the evaluation year. HAM simulations are conducted for wall configurations with an exposure height of 10 m. The minimum rain temperature is considered to be -2°C, meaning that below this temperature rain falls as snow.



### *A. Exterior Boundary Conditions*

#### *1) Ghent*

The measured meteorological data at four locations in Ghent, originating from the MOCCA project, are addressed to analyse the influence of the urban heat island (UHI) effect on retrofitted solid masonry wall assemblies. The project MOCCA, MOnitoring the City's Climate and Atmosphere, was initiated by the Department of Physics and Astronomy of Ghent University to study the UHI in Ghent (Caluwaerts et al. 2016). High-accuracy measurement stations are monitoring the urban climate since July 1st 2016. The weather stations are spread over the different landscapes characteristic for a middle-sized European city: the rural area around Ghent (Melle), the port environment with industrial activity (Honda), the suburbia covered by (semi-) detached housing and green zones (Wondelgem), and a broad urban street canyon in the city centre (Provinciehuis) (figure A.1 as part of the Supplementary Data available online). An urban park (Plantentuin) and narrow street canyon (St. Bavo School) are part of the MOCCA project as well, but are not considered in this study. Each MOCCA station uses identical professional sensors to measure different meteorological parameters at 2 m height. Data are available at a 1 minute temporal frequency. Please refer to Caluwaerts et al. (2016) for more detailed information about the sensors and the locations of the MOCCA network. This study considers observations of the actively ventilated temperature, relative humidity, wind velocity and direction, and precipitation for one particular year (July 1st 2016 until June 30th 2017). This means that no mean nor

extreme evaluation year is considered. Note that for this reason, this study should be considered as a sensitivity test to evaluate the impact of intra-urban climatic differences. No absolute damage risks can be assessed.

Wind velocity data are extrapolated from 2 m to 10 m using the Power Law as provided in Straube and Burnett's (2000) formula to calculate wind-driven rain (WDR) load. Direct and diffuse shortwave radiation data, as well as cloud cover, are collected from the Meteonorm database (Meteotest 2018) using the measurement station of Uccle, 50 km South East of Ghent. To incorporate longwave radiation in the HAM simulations, sky temperature is computed and ground temperature is set equal to air temperature, as suggested in the Delphin user manual (Nicolai and Grunewald 2006).

*2) Europe*

To analyse the distribution of critical freeze-thaw-cycles across Europe data are collected from the Meteonorm database by the Swiss company Meteotest Gonossenschaft (2015, 2018), one of the few sources providing statistical average weather files at a global range. The data contain either measured or interpolated values between different measure stations. The process to select the 36 locations is based upon climate zone, categorized in accordance to Troll and Paffen (1980), geographical situation and spread, and availability of measured data. Furthermore, each climate zones is represented by one location, i.e. Mediterranean climates with humid winters and dry summers (Madrid), maritime climates with mild winters (De Kooy), submaritime climates (Vienna), subcontinental climates (Stockholm), maritime boreal climates (Bodø) and continental boreal climates (Sodankylä). The analysis of the European freeze-thaw pattern uses a Typical Meteorological Year of the period 2000-2009 ($TMY_{2000\text{-}2009}$). To investigate the impact of climate change two TMY are studied, one for each period 1961-1990 and 2000-2009. Within each individual period no evolution of global warming is considered.



Whereas a Test Reference Year (TRY) is one actual average year selected from a database containing measured weather data (NCDC 1976; A.L.S. Chan et al. 2006), a TMY is a synthetized year combining averages from multiple years by means of statistical algorithms (Hall et al. 1978; NCDC 1981; A.L.S. Chan et al. 2006; Meteotest 2015). Intermediate hourly values of TMY are generated based on monthly averages of different climatic parameters using a stochastic model. The generated hourly values have identical statistical properties as the monthly data. Furthermore, the computational algorithms guarantee the compatibility between the different climatic parameters. Note that only average years are evaluated in this study, not including extreme events and return periods.

*B. Interior Boundary Conditions*

Interior boundary conditions per location are generated by Delphin in function of outdoor air temperature based upon the standard ISO 13788 (Nicolai and Grunewald 2006). The generated indoor air temperature and relative humidity range respectively between 20-25°C and 35-65%.

### C. *Wall Assembly*

The solid masonry wall assembly, before retrofitting, is composed of 300 mm historical brick ('Historical Brick Cluster 4' originating from the Delphin Library) and 12 mm gypsum plaster at the interior side. Please refer to figure A.2 and table A.1 for the material properties of the considered masonry. After retrofitting the gypsum plaster is replaced by 150 mm mineral wool, a vapour barrier and 12 mm gypsum board. To reduce the computational cost, the masonry is assumed to be homogeneous brick stone, a simplification found to be acceptable by Vereecken and Roels (2013) for walls subjected to real climate conditions.

### D. *Freeze-thaw criterion*

In this study, the number of critical freeze-thaw-cycles ($FTC_{crit}$) resulting from HAM simulations is considered to assess the durability of historical masonry against frost action. One $FTC_{crit}$ is counted each time the ice mass density exceeds a predetermined value, i.e. the critical moisture saturation degree ($S_{crit}$), and thawing is considered when the ice mass density drops below this value. The maximum number of $FTC_{crit}$ across the masonry is the considered number of $FTC_{crit}$. Furthermore, the freezing temperature at each point in the porous material is calculated using the Kelvin equation. In this way, the freezing point depression is taken into account, as mentioned in the introduction.

As there is no $S_{crit}$ available for the masonry in this study, the ice volume rate level of 25 % of the open porosity is the arbitrarily chosen criterion, based upon Straube and Schumacher (2010). In the case of 'Historical Brick Cluster 4' (Delphin Library) the critical ice mass density is equal to 82.5 kg/m³. Note that the criterion is chosen on the safe side and can only be used to quantitatively assess the number of $FTC_{crit}$ for varying climate conditions, not as an absolute pass/fail criterion.



### E. *Criterion mould growth*

The threshold values for the initiation of mould growth are 80 % relative humidity and a temperature higher than 0°C during sufficiently long exposure time, typically longer than one month (Hukka and Viitanen 1997).

### F. *Climatic Index*

The Climatic Index (CI), introduced by Zhou et al. (2016), is the ratio between the wetting and drying potential of a wall assembly (equation 1). The annual WDR load is the considered wetting potential, whereas the drying potential is described as the ability for the exterior air to remove moisture from the façade surface by evaporation. In this study, the annual outward vapour (diffusion) flux at the exterior masonry surface represents the potential evaporation. A CI ranging between 0 and 1 indicates a larger drying than wetting potential of the wall assembly, whereas a CI exceeding 1 implies the reverse.

(1) $$Climatic\ Index = \frac{annual\ wind\ driven\ rain\ load}{annual\ potential\ evaporation}$$

## III. CRITICAL ORIENTATION IN DURABILITY ASSESSMENT

### *A. Ghent*

To assess the durability of building materials the worst-case-scenario should be considered. For this reason it is important to determine the critical wall orientation. This section evaluates the difference in durability between two wall orientations, i.e. the South West (SW) at 225° (North = 0°, East = 90°) and the North West (NW) at 315°, of retrofitted solid masonry wall assemblies in Melle. The wall orientation facing the SW receives the highest annual wind-driven rain (WDR) load (79.6 l/m²), whereas the NW represents the wall orientation at the shadow side of the building receiving a high annual WDR load (51.4 l/m²), but lacking direct shortwave radiation in winter. Despite, the largest annual WDR load for the SW wall, the moisture content (MC) in the NW wall is higher in January, prior to freezing temperatures in the masonry, due to one particular high intensity WDR event (figure 1b and 1c and figure A.3). Beside the high wetting load during this event, the drying rate is lower in the NW shadow wall compared to the SW wall. The exterior surface of the SW wall is able to dry during shortwave radiation, lowering the MC at the exterior surface (figure A.3). At night, the MC of the pore matrix redistributes to restore the moisture balance. This increased drying rate does not occur in the NW wall to the same extent.

In the SW wall assembly there is no occurrence of critical freeze-thaw-cycles ($FTC_{crit}$) during the evaluation year, whereas the NW wall assembly sustains 7 $FTC_{crit}$ (figure 2). This is related to the high intensity WDR event prior to freezing, the lower temperatures, and the lower drying rate in the NW wall assembly. It can be concluded that the wall orientation receiving the highest annual WDR load does not necessarily sustain the most $FTC_{crit}$.

The second damage mechanism in this study is mould growth, both at the inner surface of the wall assembly (on the gypsum layer) and the interior masonry surface. Whereas there is a considerable difference in durability considering the freeze-thaw risk, there is no significant sensitivity due to orientation for mould growth.

### *B. Europe*

To determine the critical orientation for the European locations the annual WDR load according to Straube and Burnett (2000) is calculated for 16 orientations at 22.5°-intervals. The WDR loads are listed in descending order and the 8 highest values provide the orientations for HAM simulations. In other words, for 8 out of 16 orientations receiving the highest WDR loads, simulations are carried out. Further, simulation results are listed in descending order in function of the maximum number of $FTC_{crit}$ across the masonry. Per location, the orientation sustaining the most $FTC_{crit}$ is the considered critical orientation. For locations that undergo no $FTC_{crit}$ no orientation is considered. The critical orientations, corresponding WDR load and $FTC_{crit}$ are listed in table A.3.

When analysing the results, a large differentiation between the critical orientations is observed. The critical orientation is not consequently equal to the orientation having the highest annual WDR load. Only for 13% of the locations during $TMY_{2000\text{-}2009}$,

the critical orientation is ranked first in the list of descending WDR loads, whereas 33% is ranked in the top 3. For $TMY_{1961-1990}$, these values are respectively 20% and 40%. Note that locations receiving high WDR loads provide more predictable results, probably related to the high absorbed moisture content. Similarly to walls in Melle (Ghent), it can be concluded that the critical orientation concerning frost action does not only depend on the annual WDR load. More study into this domain is recommended to support future research.

## IV. Influence of interior retrofit on solid masonry

### *A. Ghent*

The influence of an interior retrofit on the number of critical freeze-thaw-cycles ($FTC_{crit}$) in solid masonry is assessed for a NW orientated wall assembly in Melle The temperature and heat flux at the interior surface are, as expected, considerably reduced after retrofitting. Whereas the lowest temperature at the interior masonry surface is initially 11.8°C, after interior retrofitting the temperature at this surface reaches the freezing point. This means that temperatures favourable for $FTC_{crit}$ occur deeper in the masonry after retrofitting.

Figure 1a and 1c illustrate the moisture content (MC) in both wall assemblies. During wind-driven rain (WDR) events moisture infiltrates in the masonry where it is stored until conditions are favourable for moisture dissipation. For uninsulated walls, this happens either to the exterior climate or to the interior climate. The exterior surface is able to dry quickly in between WDR events, and the interior masonry surface remains dry throughout the entire evaluation year.

The interior insulation, on the other hand, restricts drying to the indoor climate and reduces the masonry's temperature, both leading to a considerably wetter and colder masonry (figure 1). In contrast to the uninsulated wall assembly, the MC at the interior masonry surface remains high throughout the year and the exterior surface remains wet for longer durations in between WDR events, meaning that the outer 50 mm of the masonry is prone to $FTC_{crit}$.

During the evaluation year, there is no occurrence of $FTC_{crit}$ in the wall assembly before retrofitting, whereas the retrofitted wall assembly sustains 7 $FTC_{crit}$ at a critical depth of 0.5 mm and 25 mm from the exterior surface (figure 2). Besides, the deepest $FTC_{crit}$ reaches 257.3 mm inside the masonry. This is both related to the lower drying rate of the masonry due to the elimination of one drying surface, and the reduced temperature in deeper parts of the masonry because of the interior insulation.

Along with frost action, mould growth as well can influence the durability of interior retrofitted solid masonry and form a threat to the indoor air quality. At the interior surface of the wall assembly (gypsum layer), favourable conditions for mould germination do not occur during the evaluation year in both wall assemblies (figure A.4). There is no increase in mould risk after retrofitting. The interior masonry surface, on the other hand, is prone to the initiation of mould growth before and after retrofitting, because 80% relative humidity and a temperature of 0°C are exceeded longer than one month in both wall assemblies (figure A.4). According to the mould index, 0.08 and 3.41 respectively before and after retrofitting, there is only a

potential risk for mould growth in the retrofitted case as mould index 1 is considered to initiate mould germination. However, both methods suggests an increased the mould risk after retrofitting the solid masonry. Note that it is uncertain whether mould growth is possible due to the airtightness of the wall assemblies, and whether the indoor air quality is endangered in the presence of a vapour barrier. As more research is required in this domain, mould growth will not be analyses further in this study.

### *B. Europe.*

Similar conclusions are valid for the influence of interior retrofitting on the freeze-thaw risk in other European regions. Whereas before retrofitting $FTC_{crit}$ occur only at 14% of the selected locations during the $TMY_{2000\text{-}2009}$, after retrofitting this becomes 47%.

## V. FREEZE-THAW BEHAVIOUR OF INTERIOR RETROFITTED SOLID MASONRY: THREE SCALES

### *A. Resolution of the city: Ghent*

To assess the influence of the urban climate on the number of critical freeze-thaw-cycles ($FTC_{crit}$), a NW orientated retrofitted solid masonry wall assembly is evaluated at the following locations: Melle situated in the rural area around the city, Honda located in the port, Wondelgem as part of the suburbia and Provinciehuis situated in the city centre.

Firstly, the weather data are compared for the different urban locations. In agreement with the urban heat island (UHI) phenomenon, the minimum, maximum and average air temperature are higher in Provinciehuis than in Melle (table A.2). The largest difference is respectively 1.46°C between the annual maximum temperatures versus 3.14°C between the minimum temperatures. Further, the daily maximum temperatures vary less than the daily minima, as the UHI effect is primary related to the reduced night time cooling rather than a higher heating degree during the day (Oke 1982; Arnfield 2003).

The particular year of data used is exceptionally dry with an annual precipitation is 544.8 mm in Melle and 557.5 mm in Uccle, whereas the average annual precipitation in Uccle is 852.4 mm according to the Royal Meteorological Institute of Belgium (KMI 2016; KMI 2017). Note that Plantentuin (the urban park) is not considered in this study as the precipitation is underestimated due to the shading by trees and leaves in the rain gauge. Furthermore, St. Bavo School is not analysed as only one location in the city centre is considered.

Wind direction at a height of 2 m is strongly influenced by surrounding obstacles and buildings, especially in urbanized areas. Measurements at locations only a few meters apart can entail different results. As the wind direction measurements in Melle, located in an open landscape, are in accordance to the synoptic wind direction, these wind direction measurements are used for all locations. This adaptation is justified as the direction of rain droplets is determined in higher air layers, independently from the local wind direction near the ground (Blocken and Carmeliet 2004).

The number of hours during which freezing temperatures occur, provides the first indication concerning the freezing behaviour at the different locations (table A.2). Melle is characterized by the longest frost duration, followed by Wondelgem

and Honda, whereas the least hours of frost occur in Provinciehuis. Further, the number of freeze-thaw-cycles ($FTC_{crit}$) crossing 0°C based upon minute data is provided. As short FTC are not critical for the masonry, only freeze-thaw events having a duration longer than 13 hours and 12 minutes (13h12m) are considered. The period of 13h12m is selected as this corresponds to the minimal in Melle to reach a threshold temperature of -5°C, based upon the assumption that moisture in small pores freezes at temperatures well below 0°C (Walder and Hallet 1985, Straube and Schumacher 2006, Zhou et al. 2017). In decreasing order, the number of FTC is the highest in Melle, Honda, Wondelgem and Provinciehuis. Additionally, the number of FTC longer than 13h12m and preceded by at least 2 mm of precipitation during the previous 24 hours is assessed: three FTC occur in Melle and Wondelgem, two FTC in Honda, and one FTC in Provinciehuis. These results indicate that the freeze-thaw risk is the highest in the rural area of Ghent, whereas the least $FTC_{crit}$ are expected in the city centre. Note that the threshold value of -5°C is arbitrarily chosen and can vary depending on material properties. Besides, for a threshold temperature of -3°C similar results are obtained.

Analysing the weather data provides a first estimation about the difference in freeze-thaw action between the locations in Ghent. However, HAM simulations, taking into account wall assembly, orientation, material properties etc, are needed to provide detailed results. These simulations demonstrate that the exterior surface temperature of the masonry generally follows the outdoor air temperature which indicates that the UHI effect is experienced in the wall assembly as well. However, the exterior surface temperature does not only depend on air temperature, but also on the solar radiation and the longwave radiation exchange with the sky and surrounding ground.

The wind-driven rain (WDR) load, function of horizontal precipitation and wind velocity, differs considerably in Melle, Honda, Wondelgem and Provinciehuis, respectively 51.4 l/m², 24.5 l/m², 8.1 l/m² and 2.6 l/m². Because the horizontal precipitation is similar at all locations (table A.2), the large differences are related to the variation in wind velocity as a result of land cover and terrain roughness. The wind velocity in the open landscape of Melle is significantly higher than in the built-up region of the (sub)urban environment of Wondelgem and Provinciehuis, resulting in a large differentiation in WDR load. Note that, due to the presence of a row of trees in the proximity of the MOCCA station in Honda, the WDR load for this location is possibly underestimated in the months prior to February 2017.

The moisture load in the pore matrix of the masonry does not only depend on the wetting potential, but relies on drying capacity as well. As this is a complex phenomenon depending on many (local) factors, the drying capacity is not assessed directly in this study. However, the relative moisture load between the different wall assemblies is assessed by the Climatic Index (CI), i.e. the ratio between the annual WDR load and potential evaporation (X. Zhou et al. 2016), as introduced in section 2. The CI of the four locations in Ghent decreases in the same order as the WDR load and the general moisture content (MC) in the masonry (figure 1c, 1d, 1e and 1f), i.e. Melle, Honda, Wondelgem and Provinciehuis. The maximum MC at the exterior surface is respectively 234.9 kg/m³, 180.5 kg/m³, 148.6 kg/m³ and 66.3 kg/m³. The MC in wall assemblies is maximal in Melle as this location receives the highest wetting load. The exterior surface sustains large peaks in MC during WDR events, the MC

remains high for longer durations in between WDR events during winter, and moisture penetrates deeper into the masonry. In winter, the critical MC is exceeded for longer periods of time. Note that the constant MC in January is related to the presence of ice mass. Honda, Wondegem and Provinciehuis receive respectively 47.7%, 15.8% and 5% of the annual WDR load of Melle.

The decrease in ice mass density follows the decrease MC of the masonry, as illustrated in figure 3. In all four wall assemblies ice crystallization and thawing occur after a certain delay in deeper parts of the masonry. In Melle, the maximum ice mass density is reached deep in the wall and partial freezing occurs up to the interior masonry surface, whereas ice crystallization in the wall assembly in Provinciehuis does not reach beyond a depth of 150 mm. The maximum values of ice mass density are 99.9 kg/m³, 62.4 kg/m³, 53.4 kg/m³ and 31.1 kg/m³, respectively in Melle, Honda, Wondelgem and Provinciehuis. Only in Melle the critical ice mass density of 82.5 kg/m³ is exceeded, and thus this is the only location sustaining $FTC_{crit}$ during the evaluation year.

Although, the only wall assembly sustaining $FTC_{crit}$ is situated in Melle, i.e. 7 $FTC_{crit}$, the freeze-thaw risk and depth is probably decreasing in the following order based upon ice mass density: Melle, Honda, Wondelgem and Provinciehuis. However, it can be concluded that there is a decrease in number of $FTC_{crit}$ in the city centre compared to the rural area during the evaluation year. Note that the assumptions made in the weather data analysis concerning the freeze-thaw risk at the different locations are only correct to some extent. HAM simulations indicate that the freeze-thaw risk in Wondelgem has been overestimated, as the weather data analysis does not take into account the WDR load, wall assembly, orientation, solar radiation etc. It can be concluded that the freeze-thaw risk not only depends on the UHI effect, but it is also strongly influenced by WDR load.



*B. Resolution of the continent: Europe*

Prior to the evaluation of climate change on the freeze-thaw behaviour of interior retrofitted solid masonry walls, the current freeze-thaw pattern is mapped and analysed using the $TMY_{2000\text{-}2009}$. The number of critical freeze-thaw-cycles ($FTC_{crit}$) across Europe is illustrated in figure 4a, whereas the number of $FTC_{crit}$ over the thickness of the masonry at the representative locations is illustrated in figure 5a. Southern Europe is categorized as a Mediterranean climate with humid winters and dry summers, a sub-category of the warm temperate climates. This climate zone is represented by Madrid, characterized by a wind-driven rain (WDR) load of 11 l/m² and a Climatic Index ($CI_{Oct\text{-}Mar}$) (as described in *section 2*) between October and March of 0.69, indicating a lower moisture load than other parts of Europe (table 1b). During WDR events only the outer layer of the masonry is wetted and moisture is able to dissipate in the masonry quickly in between WDR events. Besides, the climate does not sustain many FTC crossing 0°C air temperature and there is only one FTC crossing 0°C based upon daily average temperature. Retrofitted masonry wall assemblies in Madrid do not sustain $FTC_{crit}$ during the $TMY_{2000\text{-}2009}$ (figure 4a and 5a). Although, the

moisture load in some other Mediterranean locations is higher than in Madrid, temperatures are often too high for $FTC_{crit}$ to occur.

The cool temperate climates are situated to the North of the warm temperate climate zone. The maritime climate with mild winters is represented by De Kooy having an annual WDR load of 83.7 l/m², a $CI_{Oct-Mar}$ of 1.00, and sustaining two FTC crossing 0°C air temperature (daily) (table 1b). There are two $FTC_{crit}$ at a depth of 10 mm and $FTC_{crit}$ do not occur beyond this depth (figure 4a and 5a). The occurrence of $FTC_{crit}$ in this climate zone typically depends on the sequence of weather events, such as WDR intensity and duration, the rate of temperature decrease after WDR events etc. Wall assemblies receiving a higher WDR load do not necessarily sustain more $FTC_{crit}$.

However, there are locations in the maritime climate with mild winters for which the number of $FTC_{crit}$ depends on the number of FTC in the climate. In these cases, the WDR load is significantly higher than other locations in the temperate climate zone, higher than 160 l/m², resulting in a moisture content (MC) exceeding the critical MC for long periods of time in winter. Examples are Bergen and Belmullet, respectively sustaining 40 and 2 $FTC_{crit}$ (figure 4a). Note that the latter location only sustains 2 FTC crossing 0°C air temperature.

The submaritime climate is situated more land ward, but still influenced by the Atlantic Ocean. A wall assembly in Vienna receives a WDR load of 30.3 l/m², has a $CI_{Oct-Mar}$ of 0.95 and sustains 9 FTC crossing 0°C air temperature (daily) (table 1b). Although only the outer surface of the masonry is wetted during WDR events, the wall assembly sustains 3 $FTC_{crit}$ during the $TMY_{2000-2009}$ at 1.9 mm, but $FTC_{crit}$ do not occur beyond this depth (figure 4a and 5a). Even though the air temperature during WDR events is higher than 0°C, the surface can be frozen due to the longwave radiation exchange with the sky and ground. During these events, $FTC_{crit}$ can occur, but the depth of $FTC_{crit}$ remains shallow. This phenomenon does occur in other climate zones across Europe as well.

The subcontinental climate zone, North East of the submaritime climate zone, is represented by Stockholm. As in the (sub)maritime climate zone, the number of $FTC_{crit}$ in the subcontinental climate zone depends on the sequence of weather events. However, the occurrence of $FTC_{crit}$ is slightly higher than the other cool temperate climates. Stockholm is characterized by a WDR load of 34.4 l/m² and $CI_{Oct-Mar}$ of 0.93, both similar to Vienna, and the number of FTC crossing 0°C air temperature (daily) is 11 (table 1b). A retrofitted solid masonry wall assembly in Stockholm sustains two $FTC_{crit}$ at 0 mm to 3.6 mm, the largest critical freeze-thaw depth (figure 4a and 5a). $FTC_{crit}$ occur at a larger depth than in wall assemblies in Vienna, but do not reach the freeze-thaw depth of De Kooy.

In Northern Europe the cold temperate boreal climates are situated, characterized by colder temperatures and limited shortwave radiation during winter. The boreal maritime climate is represented by Bodø, receiving a WDR load of 164.8 l/m², a $CI_{Oct-Mar}$ of 1.04 and 18 FTC crossing 0°C air temperature (daily) (table 1b). The number of $FTC_{crit}$ during the $TMY_{2000-2009}$ is 42 at the exterior surface, the highest number of $FTC_{crit}$ in Europe, and $FTC_{crit}$ reach throughout the entire masonry (figure 4a and 5a). As in the maritime climate with mild winter, there are two trends in this climate zone. Either the number of $FTC_{crit}$

depends on the number of FTC in the climate for locations receiving a high WDR load, for instance in Bodø, or the number of FTC depends on the sequence of weather events.

The boreal continental climate zone, on the other hand, does not sustain any $FTC_{crit}$ during the $TMY_{2000-2009}$, as the WDR load during winter is negligible. The WDR load in Sodankylä is 12.5 l/m², of which only 3.5 l/m² is absorbed between October and March, the $CI_{Oct-Mar}$ is 0.43, and the number of FTC crossing 0°C (daily) is 16, only occurring in early autumn and late spring (table 1b, figure 4a and 5a).

Across the evaluated part of Europe three trends concerning the occurrence of $FTC_{crit}$ are distinguished: (i) In maritime climates, characterized by a high WDR load, the number of FTC primary depends on the number of FTC in the climate as the critical MC is exceeded during long periods, (ii) In temperate climates, receiving a lower WDR load, the number of $FTC_{crit}$ depends on the sequence of weather events, such as WDR intensity, frequency and duration, drying potential, surface temperature, freezing rate following WDR events etc. (iii) In the Mediterranean and continental boreal climates there is no occurrence of $FTC_{crit}$, either because there are few FTC in the climate or the moisture load is particularly low and the MC does not exceed the critical MC.

*C. Temporal resolution: recorded climate change across Europe*

The change of the number of critical freeze-thaw-cycles ($FTC_{crit}$) across Europe based upon observed climate change is illustrated in figure 4b, whereas the evolution in $FTC_{crit}$ over the thickness of the masonry at the representative locations is illustrated in figure 5b. In the Mediterranean climate zone there is no change in the freeze-thaw risk, as the number of $FTC_{crit}$ remains zero for both $TMY_{1961-1990}$ and $TMY_{2000-2009}$ (figure 4b and 5b). In Madrid, WDR load decreases between both TMY and the number of FTC crossing 0°C based upon daily average temperature remains one (table 1a and 1b).

In the maritime climate zone with mild winters there is in general a decrease in the number of $FTC_{crit}$ (figure 4b and 5b). In De Kooy, the WDR load decreases between 142.0 l/m² and 83.7 l/m² whereas $CI_{Oct-Mar}$ remains the same, indicating a decreasing wetting potential of the wall assembly. Further, as the average temperature increases, there is a decrease of FTC crossing 0°C air temperature (daily) (table 1a and 1b). The number of $FTC_{crit}$ in De Kooy decreases from four to two, the freeze-thaw depth moves from 52.8 mm to 10 mm, and the $FTC_{crit}$ depth changes from 20 mm to 10 mm. Whereas there is a negative increase of the number of $FTC_{crit}$ beyond 10 mm, the number of $FTC_{crit}$ is neutral close to the exterior surface.

There is no clear trend in the submaritime climate zone, possibly related to the presence of the Alps (figure 4b and 5b). Grossi et al. (2007) indicate that sites having a high altitude potentially sustain an increasing number of $FTC_{crit}$ which is the case for St.-Gallen (779 m a.s.l.). In Vienna, the number of $FTC_{crit}$ increases from zero to three. As mentioned before, $FTC_{crit}$ only occur in the outer 1.9 mm of the masonry. WDR load increases between the two TMY and the percentage of WDR load absorbed between October and March increases from 38.4 % to 53.9 % (table 1a and 1b). Although, there is an increase in sub-zero

average temperatures in winter, presumably leading to more fluctuations around the freezing point (Grossi et al. 2007), the number of FTC crossing 0°C air temperature (daily) decreases in Vienna.

In the subcontinental climate zone the number of $FTC_{crit}$ decreases in three of the five locations (figure 4b and 5b), but Grossi et al. (2007) indicate the liability of major changes in this region based upon long-term simulations. In Stockholm, the number of $FTC_{crit}$ decreases from five to two, and the freeze-thaw depth shifts from 13.5 mm to 3.6 mm. As in Vienna, the distribution of WDR load shifts more towards the winter months, i.e. from 32.0 % to 52.6% between October and March (table 1a and 1b). Further, there is an increase of sub-zero average temperatures and a decrease of FTC crossing 0°C air temperature (daily).

In the maritime boreal climate zone, the number of $FTC_{crit}$ decreases in two of the locations, whereas there is an increase of 21 $FTC_{crit}$ in Bodø (figure 4b and 5b). This city too sustains an increase in WDR load and percentage of WDR load between October and March, i.e. 56.3 % to 76.8 % (table 1aand 1b). Sub-zero average temperatures increase as well, but the number of fluctuations around 0°C air temperature (daily) decreases. The number of $FTC_{crit}$ increases from 21 to 42, the largest raise across Europe. The freeze-thaw depth reaches the interior masonry surface for both TMY and the critical depth moves from 45 mm to the exterior surface. The largest increase of $FTC_{crit}$ occurs in the outer 100 mm of the masonry, which is the part of the masonry most sensitive to the increased wetting load.

In the continental boreal climate some locations sustain a decrease of one $FTC_{crit}$, whereas the number of $FTC_{crit}$ in other locations remains zero, as in Sodankylä (table 1a and 1b, figure 4b and 5b).

In 14 % of the locations across Europe there is an increase of the number of $FTC_{crit}$ in retrofitted solid masonry wall assemblies, in 47 % the number of $FTC_{crit}$ decreases, in 3 %, sustaining at least one $FTC_{crit}$, the number remains neutral, and in 36 % the number of $FTC_{crit}$ remains zero. In accordance to Grossi et al. (2007) there is a general decrease of $FTC_{crit}$ in temperate Europe. Locations having a northern latitude or high altitude potentially sustain an increasing number of $FTC_{crit}$. Additionally there can be observed that this is more likely for locations receiving an increasing WDR load during winter months. Note that this study only considers TMY, not including extreme events or return periods.

## VI. Conclusion

Based on urban heat island observations in Ghent, it can be concluded that this phenomenon has a significant impact on the freeze-thaw risk. However, the difference in wind-driven rain (WDR) load, i.e. 51.4 l/m², 24.5 l/m², 8.1 l/m² and 2.6 l/m², in respectively Melle, Honda, Wondelgem and Provinciehuis, induces the main difference. For the evaluation year a clear decrease in the freeze-thaw risk and mould growth is found in the more urbanized landscapes of Ghent. Although, the retrofitted solid masonry wall assembly in the rural area is the only one sustaining critical freeze-thaw-cycles ($FTC_{crit}$), the freeze-thaw risk is supposedly decreasing in the following order: rural area, port site, suburbia and city centre of Ghent. Note that absolute values of $FTC_{crit}$ are sensitive to the arbitrary chosen critical ice volume rate of the masonry, which is probably on the safe side.

Across Europe three trends concerning the occurrence of $FTC_{crit}$ are distinguished, based upon a Typical Meteorological Year of the period 2000-2009 ($TMY_{2000-2009}$): (i) In maritime climates, sustaining a high WDR load, the number of $FTC_{crit}$ primary depends on the number of FTC in the climate. (ii) In temperate climates, including the city of Ghent, receiving a lower WDR load, the number of $FTC_{crit}$ depends on the sequence of weather events. (iii) In the Mediterranean and continental boreal climates there is no occurrence of $FTC_{crit}$.

Across Europe, 14 % of the locations undergo an increase in number of $FTC_{crit}$, 47 % of the locations sustain a decrease, 3 % of the locations, sustaining at least one $FTC_{crit}$, remain neutral, and 36 % of the locations do not sustain $FTC_{crit}$ between the $TMY_{1961-1990}$ and $TMY_{2000-2009}$.

Furthermore, in accordance with the study of Grossi et al. (2007) retrofitted solid masonry wall assemblies in the temperate climate zone of Europe generally experience a decrease in number of $FTC_{crit}$, whereas locations having a Northern latitude or high altitude potentially undergo an increase. In addition to Grossi et al. (2007), by taking into account the wall assembly and the critical orientation per location, the moisture load is considered in the freeze-thaw criterion. Therefore, the distribution of the WDR load across the year is of importance when assessing the freeze-thaw risk. An increasing number of $FTC_{crit}$ is more likely for locations experiencing an increased WDR load during winter.

The analysis considering the urban climate of Ghent evaluates one particular year of measured data, whereas the study on the (changing) pattern of $FTC_{crit}$ across Europe is based upon the use of TMY. The selection of climatic years in both analyses may have significant implications. It may be of interest to address extreme years, multiyear climate data and future climate projections when performing hygrothermal risk assessment.

Nevertheless, the study shows that the urban environment and climate change both impact the durability of the building envelope. Therefore future research considering the degradation of building materials due to climate change would benefit from using high resolution climate projections that include the effects of the urban environment. Furthermore, the research illustrates that conclusions on the freeze-thaw behaviour of wall assemblies strongly depend on the studied location and resolution.



## ACKNOWLEDGEMENTS

Tim De Kock, postdoctoral research fellow of the Research Foundation – Flanders (FWO), and Klaas Calle, doctoral research fellow of the FWO (SBO-1S45416N), would like to acknowledge its support.

## REFERENCES

Adan, O.C.G. 1994. On the fungal defacement of interior finishes. PhD thesis, Eindhoven University of Technology, Eindhoven.

Arnfield, A. J. 2003. Review two decades of urban climate research : A review of turbulence, exchanges of energy and water, and the urban heat island. International Journal of Climatology, **23**: 1–26. doi:10.1002/joc.859.

Blocken, B., and Carmeliet, J. 2004. A review of wind-driven rain research in building science. Journal of Wind Engineering and Industrial Aerodynamics, **92**(13): 1079–1130. doi:10.1016/j.jweia.2004.06.003.

Bohnenstengel, S.I., Hamilton, I., Davies, M., and Belcher, S.E. 2014. Impact of anthropogenic heat emissions on London's temperatures. Quarterly Journal of the Royal Meteorological Society, **140**: 687-698. doi:10.1002/qj.2144.

Caluwaerts, S., Termonia, P., Hamdi, R., Duchêne, F., Berckmans, J., Degrauwe, D., and Wauters, G. 2016. Monitoring the urban climate of the city of Ghent, Belgium. International Association for Urban Climate, **61**: 15-20.

Chan, A. L. S., Chow, T. T., Fong, S. K. F., and Lin, J. Z. 2006. Generation of a typical meteorological year for Hong Kong. Energy Conversion and Management, **47**(1): 87–96. doi:10.1016/j.enconman.2005.02.010.

Fagerlund, G. 1973. Critical degrees of saturation at freezing of porous and brittle materials Tid. Institutionen för byggnadsteknik, Tekniska högskolan i Lund, Lund.

Grossi, C. M., Brimblecombe, P., and Harris, I. 2007. Predicting long term freeze-thaw risks on Europe built heritage and archaeological sites in a changing climate. Science of the Total Environment, **377**(2–3): 273–281. doi:10.1016/j.scitotenv.2007.02.014.

Hall, I.J., Prairie, R.R., Anderson, H.E., and Boes, E.C. 1978. Generation of a typical meteorological year. *In* Proceedings of the 1978 annual meeting of the American Section of the International Solar Energy Society, Denver, C.O., 28-31 August 1978. International Solar Energy Society, American Section, Newark, D.E., pp. 669-671.

Hukka, A., and Viitanen, H. A. 1999. A mathematical model of mould growth on wooden material. Wood Science and Technology, **33**(6): 475–485. doi:10.1007/s002260050131.

IPCC. 2013. Climate Change 2013: The physical science basis. Contribution of Working Group I to the Fifth Assessment Report of the Intergovernmental Panel on Climate Change. Cambridge University Press: Cambridge, 1132 pp.

KMI. 2016. Klimatologisch maandoverzicht, juli/ augustus/ september/ oktober/ november/ december 2016 [pdf]. Available from http://www.meteo.be/resources/climateReportWeb/klimatologisch_maandoverzicht [accessed 5 August 2018].

KMI. 2017. Klimatologisch maandoverzicht, januari/ februari/ maart/ april/ mei/ juni 2017 [pdf]. Available from http://www.meteo.be/resources/climateReportWeb/klimatologisch_maandoverzicht [accessed 5 August 2018].

Lisø, K. R., Kvande, T., Hygen, H. O., Thue, J. V., and Harstveit, K. 2007. A frost decay exposure index for porous, mineral building materials. Building and Environment, **42**(10): 3547–3555. doi:10.1016/j.buildenv.2006.10.022.

Maiheu, B., Van den Berghe, K., Boelens, L., De Ridder, K., and Lauwaet, K. 2013. Opmaak van een hittekaart en analyse van het stedelijk hitte-eiland effect voor Gent. Report 2013/RMA/R/113, VITO, Mol, Belgium. doi:2013/RMA/R/113.

Meteotest 2015. Meteonorm Global Meteorological Database: Handbook Part I & II. Meteotest, Bern.

Meteotest. 2018. Meteonorm Features. Available from https://www.meteonorm.com/ [accessed 5 August 2018].

National Climatic Data Center (NCDC). 1976. ASHRAE Test Reference Year Reference Manual TD-9706. NCDC, U.S. Department of Commerce, Asheville, N.C.

National Climatic Data Center (NCDC). 1981. Typical Meteorological Year User's Manual, TD-9734, Hourly solar radiation – Surface meteorological Observations. NCDC, U.S. Department of Commerce, Asheville, N.C.

Nicolai, A., and Grunewald, J. 2006. Delphin 5, version 5.2, User Manual and Programme Reference.

Oke, T.R. 1979. Review of Urban Climatology 1973-1976. World Meteorological Organization: Geneva. WMO Technical Note No. 169

Oke, T.R. 1982. The energy basis of the urban heat island. Quarterly Journal of the Royal Meteorological Society, **108**: 1-24. doi:10.1002/qj.49710845502.

Sedlbauer, K. 2001. Prediction of mould fungus formation on the surface of/and inside building components. Thesis, Fraunhofer Institute for building Physics, University of Stuttgart, Stuttgart.

Stewart, I. D., and Oke, T. R. 2012. Local climate zones for urban temperature studies. Bulletin of the American Meteorological Society, **93**(12): 1879–1900. doi:10.1175/BAMS-D-11-00019.1.

Straube, J.F., and Burnett, E.F.P. 2000. Simplified prediction of driving rain deposition. *In* Proceedings of the International Building Physics Conference, Eindhoven, September 18-21 2000, pp. 375-382.

Straube, J., and Schumacher, C. 2006. Assessing the durability impacts of energy efficient enclosure upgrades using hygrothermal modeling. Journal of the International Association for Science and Technology of Building Maintenance and Monuments Preservation, Vol 2, 2006.

Straube, J.F., and Schumacher, C. 2007. Interior Insulation Retrofits of Load-Bearing Masonry Walls in Cold Climates. Journal of Green Building, **2**(2): 42–50. doi:10.3992/jgb.2.2.42.

Straube, J. F., Ueno, K., and Schumacher, C. 2011. Internal Insulation of Masonry Walls : Final Measure Guideline. Building Science Press, Building America Report-1105 (21 December 2011), 1–99, Office of Scientific and Technical Information, U.S. Department of Energy. doi: 10.2172/1048975.

Straube, J.F., Schumacher, C., and Mensinga, P. 2010. Assessing the freeze-thaw resistance of clay brick for interior insulation retrofit projects, *In* Proceedings of the Conference on Performances of Envelopes of Whole Buildings XI, Clearwater Beach, Florida, 5-9 December 2010. ASHRAE.

Troll, C., and Paffen, K.H. 1980. Jahreszeitenklimate der Erde. Berlin.

van Hove, L. W. A., Jacobs, C. M. J., Heusinkveld, B. G., Elbers, J. A., Van Driel, B. L., and Holtslag, A. A. M. 2015. Temporal and spatial variability of urban heat island and thermal comfort within the Rotterdam agglomeration. Building and Environment, **83**: 91–103. doi:10.1016/j.buildenv.2014.08.029.

Vereecken, E., and Roels, S. 2013. Hygric performance of a massive masonry wall: How do the mortar joints influence the moisture flux? Construction and Building Materials, **41**: 697–707. doi:10.1016/j.conbuildmat.2012.12.024.

Viitanen H.A., and Ojanen T. 2007. Improved Model to Predict Mold Growth in Building Materials. *In* Preceedings of the Conference on Thermal Performance of Exterior Envelopes of Whole Buildings X, Clearwater Beach, Florida, 2-7 December 2007. ASHREA.

Viitanen, H.A., and Ritschkoff, A. 1991. Mould growth in pine and spruce sapwood in relation to air humidity and temperature. Report no 221, Department of Forest Products, The Swedish University of Agricultural Sciences, Uppsala.

Walder, J.S., and Hallet, B. 1985. Theoretical model of the fracture of rock during freezing. Bulletin of the Geological Society of America, **96**(3): 336-346.

Wardeh, G., and Perrin, B. 2008. Freezing-thawing phenomena in fired clay materials and consequences on their durability. Construction and Building Materials, **22**(5): 820–828. doi:10.1016/j.conbuildmat.2007.01.004.

Wessman, L. 1997. Studies on the frost resistance of natural stone. Division of Building Materials, LTH, Lund University, Lund

World Health Organization (WHO). 2009. WHO guidelines for indoor air quality: dampness and mould. WHO Regional Office for Europe, Geneva.

WTA. 2014. Innendämmung nach WTA II - Nachweis von Innendämmsystemen mittels numerischer Berechnungsverfahren. WTA Merkblatt 6-5-14-D, WTA Publications, Pfaffenhofen.

Zhou, X., Derome, D., and Carmeliet, J. 2016. Robust moisture reference year methodology for hygrothermal simulations. Building and Environment, **110**: 23–35. doi:10.1016/j.buildenv.2016.09.021.

Zhou, X., Derome, D., and Carmeliet, J. 2017. Hygrothermal modeling and evaluation of freeze-thaw damage risk of masonry walls retrofitted with internal insulation. Building and Environment, **125**: 285–298. doi.org/10.1016/j.buildenv.2017.08.001.

## List of Abbreviations

CI: Climatic Index

FTC: freeze-thaw-cycle

HAM: Heat Air Moisture

M: Mould Index

MC: moisture content

NW: North West

RH: relative humidity

S: degree of moisture saturation

SW: South West

T: temperature

TMY: typical meteorological year

TRY: test reference year

UCL: urban canopy layer

UHI: urban heat island

WDR: wind-driven rain

*Subscripts*

Ann.: annual

Crit: critical

Jan.: January

Oct-Mar: for the period of October until March

## TABLE CAPTIONS

Table 1 Climate parameters in Vienna, De Kooy, Bodø, Stockholm, Sodankylä and Madrid, considering the $TMY_{1961\text{-}1990}$ (A) and $TMY_{2000\text{-}2009}$ (B). Note that the critical orientations of Sodankylä and Madrid, unlike other locations that sustain $FTC_{crit}$ (*section III.B*), are determined based on maximum ice mass density.

FIGURE CAPTIONS

Figure 1 Moisture mass density every 50 mm in the masonry (daily) and wind-driven rain load (WDR) (hourly): A. Melle, NW, original wall assembly, B. Melle, SW, retrofitted wall assembly, C. Melle, NW, retrofitted wall assembly, D. Honda, NW, retrofitted wall assembly, E. Wondelgem, NW, retrofitted wall assembly, and F. Provinciehuis NW, retrofitted wall assembly (10 minute data)

Figure 2 Number of freeze-thaw-cycles for the walls situated in Melle (NW): before and after retrofit

Figure 3 Ice mass density throughout the masonry in the NW-orientated retrofitted wall assembly in A. Melle, B. Honda, C. Wondelgem, and D. Provinciehuis (10 minute data)

Figure 4 The number of critical freeze-thaw-cycles ($FTC_{crit}$) for TMY 2000-2009 (A) and increase in number of $FTC_{crit}$ between TMY 1961-1990 and TMY 2000-2009 across Europe (map: Google Earth 2018)

Figure 5 The number of critical freeze-thaw-cycles ($FTC_{crit}$) for TMY 2000-2009 (A) and increase in number of $FTC_{crit}$ between TMY 1961-1990 and TMY 2000-2009 (B) in Bodø , De Kooy, Vienna and Stockholm

## SUPPLEMENTARY DATA CAPTIONS

Figure A.1 Location and land cover of the measure stations in the urban environment of Ghent (Caluwaerts et al. 2016, adapted)

Figure A.2 Functions 'Historical Brick Cluster 4': A. Sorption isotherm, B. liquid conductivity in function of moisture content, C. heat conductivity (lambda) in function of moisture content, and D. capillary pressure (logarithmic) in function of moisture content. (Delphin Material Library (5.9.5))

Figure A.3 Moisture mass density and absorbed shortwave radiation at the exterior surface of the retrofitted wall assemblies in Melle, orientated to the South West and the North West (10 minute data)

Figure A.4 Relative humidity at the interior surface of the masonry and wall assembly of the North West orientated wall in Melle: A. before retrofit and B. after retrofit (daily data)

Figure A.5 Relative humidity at the interior surface of the masonry and wall assembly of the North West retrofitted wall assembly in A. Melle, B. Honda, C. Wondelgem, and D. Provinciehuis (daily data)

Table A.1 Material properties of 'Historical Brick Cluster 4' (Delphin Material Library (5.9.5))

Table A2 Temperature, precipitation, time of frost and number of freeze-thaw-cycles ($FTC_{crit}$) in Ghent: Melle, Honda, Wondelgem and Provinciehuis

Table A.3 Climate parameters at 36 locations across Europe: critical orientation, number of critical freeze-thaw cycles ($FTC_{crit}$), annual wind-driven rain (WDR) load and average temperature in January

# TABLES

Table 1 Climate parameters in Vienna, De Kooy, Bodø, Stockholm, Sodankylä and Madrid, considering the $TMY_{1961\text{-}1990}$ (A) and $TMY_{2000\text{-}2009}$ (B). Note that the critical orientations of Sodankylä and Madrid, unlike other locations that sustain $FTC_{crit}$ (*section III.B*), are determined based on maximum ice mass density.

| | Location / Parameter | Bodø | De Kooy | Vienna | Stockholm | Sodankylä | Madrid |
|---|---|---|---|---|---|---|---|
| A | **TMY 1961-1990** | | | | | | |
| | **Orientation [°]** | 112.5 | 270 | 67.5 | 270 | 247.5 | 337.5 |
| | **Crit. FTC [-]** | 21 | 4 | 0 | 5 | 0 | 0 |
| | **FTC<0°C, hourly [-]** | 78 | 36 | 55 | 91 | 89 | 25 |
| | **FTC<0°C, daily [-]** | 21 | 5 | 13 | 16 | 10 | 1 |
| | **WDR [l/m²]** | 149.1 | 142.0 | 22.9 | 34.1 | 21.9 | 28.9 |
| | **WDR Oct-Mar. [%]** | 56.3 | 46.6 | 38.4 | 32.0 | 13.0 | 58.0 |
| | **CI [-]** | 0.99 | 1.00 | 0.78 | 0.91 | 0.77 | 0.82 |
| | **CI Oct-Mar. [-]** | 0.96 | 0.97 | 0.80 | 0.78 | 0.36 | 0.93 |
| | **Crit. Depth FTC[mm]** | 45 | 20 | / | 3.6 | / | / |
| | **Deepest crit. FTC [mm]** | 300 | 52.8 | / | 13.5 | / | / |
| | **T (mean Jan.) [°C]** | -2.2 | 2.7 | -0.7 | -2.8 | -15.1 | 5.5 |
| | **T (mean Ann.) [°C]** | 4.5 | 9.4 | 9.9 | 6.6 | -1.0 | 13.9 |
| B | **TMY 2000-2009** | | | | | | |
| | **Orientation [°]** | 112.5 | 112.5 | 67.5 | 90 | 90 | 337.5 |
| | **Crit. FTC [-]** | 44 | 2 | 3 | 2 | 0 | 0 |
| | **FTC<0°C, hourly [-]** | 69 | 18 | 45 | 83 | 104 | 32 |
| | **FTC<0°C, daily [-]** | 18 | 2 | 9 | 11 | 16 | 1 |
| | **WDR [l/m²]** | 164.8 | 83.7 | 30.3 | 34.4 | 12.5 | 11 |
| | **WDR Oct-Mar. [%]** | 126.5 | 53.6 | 16.3 | 18.1 | 3.5 | 7.0 |
| | **CI [-]** | 76.8 | 64.0 | 53.9 | 52.6 | 28.1 | 63.4 |
| | **CI Oct-Mar. [-]** | 0.99 | 1.00 | 0.84 | 0.88 | 0.62 | 0.59 |
| | **Crit. Depth FTC[mm]** | 1.04 | 1.00 | 0.95 | 0.93 | 0.43 | 0.69 |
| | **Deepest crit. FTC [mm]** | 0 | 10 | 1.9 | 0 – 3.6 | / | / |
| | **T (mean Jan.) [°C]** | 300 | 10 | 1.9 | 3.6 | / | / |
| | **T (mean Ann.) [°C]** | -0.4 | 4.5 | 0.6 | -1.0 | -11.7 | 5.2 |
| | **Orientation [°]** | 5.6 | 10.7 | 11.1 | 7.8 | 0.7 | 14.5 |

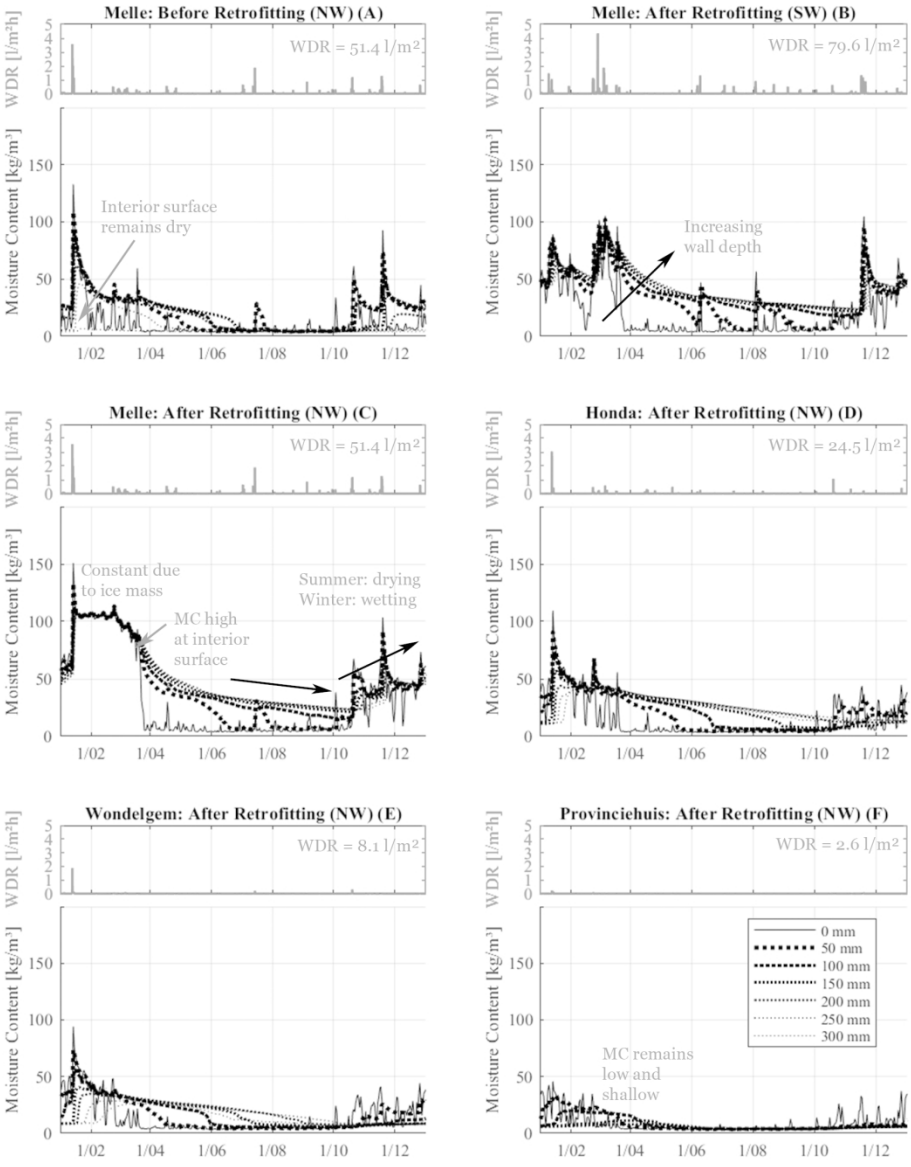


Figure 1 Moisture mass density every 50 mm in the masonry (daily) and wind-driven rain load (WDR) (hourly): A. Melle, NW, original wall assembly, B. Melle, SW, retrofitted wall assembly, C. Melle, NW, retrofitted wall assembly, D. Honda, NW, retrofitted wall assembly, E. Wondelgem, NW, retrofitted wall assembly, and F. Provinciehuis NW, retrofitted wall assembly

160x199mm (300 x 300 DPI)

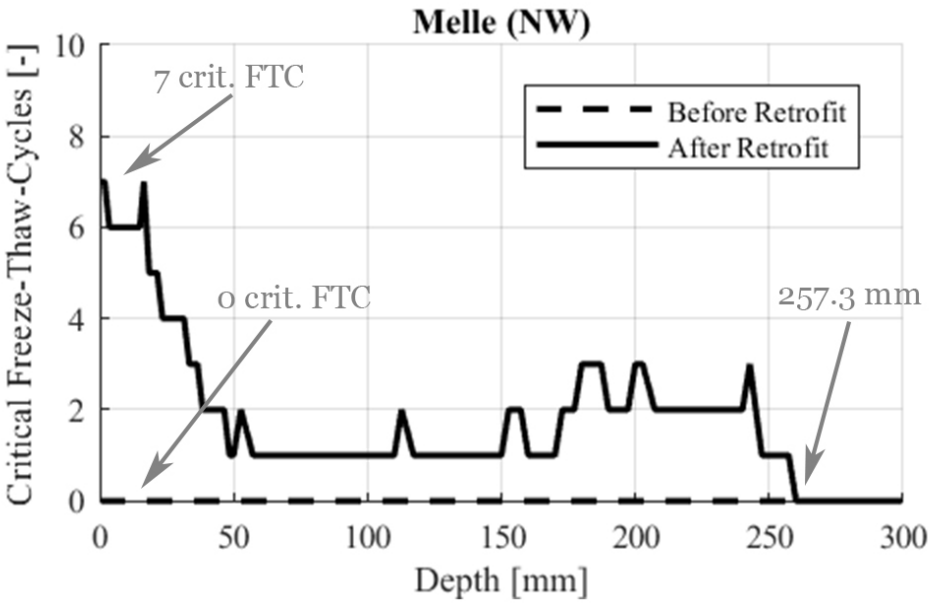


Figure 2 Number of freeze-thaw-cycles for the walls situated in Melle (NW): before and after retrofit

86x54mm (300 x 300 DPI)

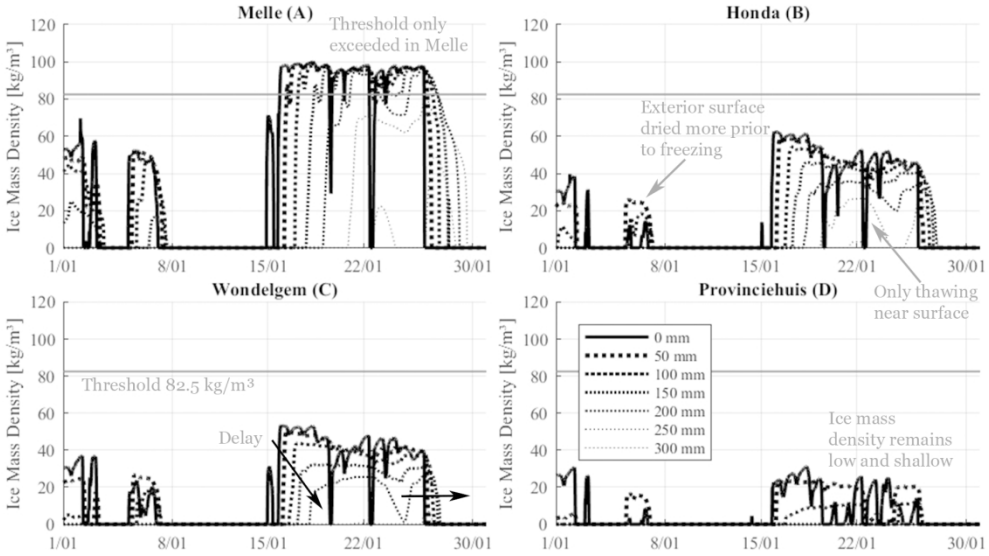


Figure 3 Ice mass density throughout the masonry in the NW-orientated retrofitted wall assembly in A. Melle, B. Honda, C. Wondelgem, and D. Provinciehuis (10 minute data)

160x88mm (300 x 300 DPI)

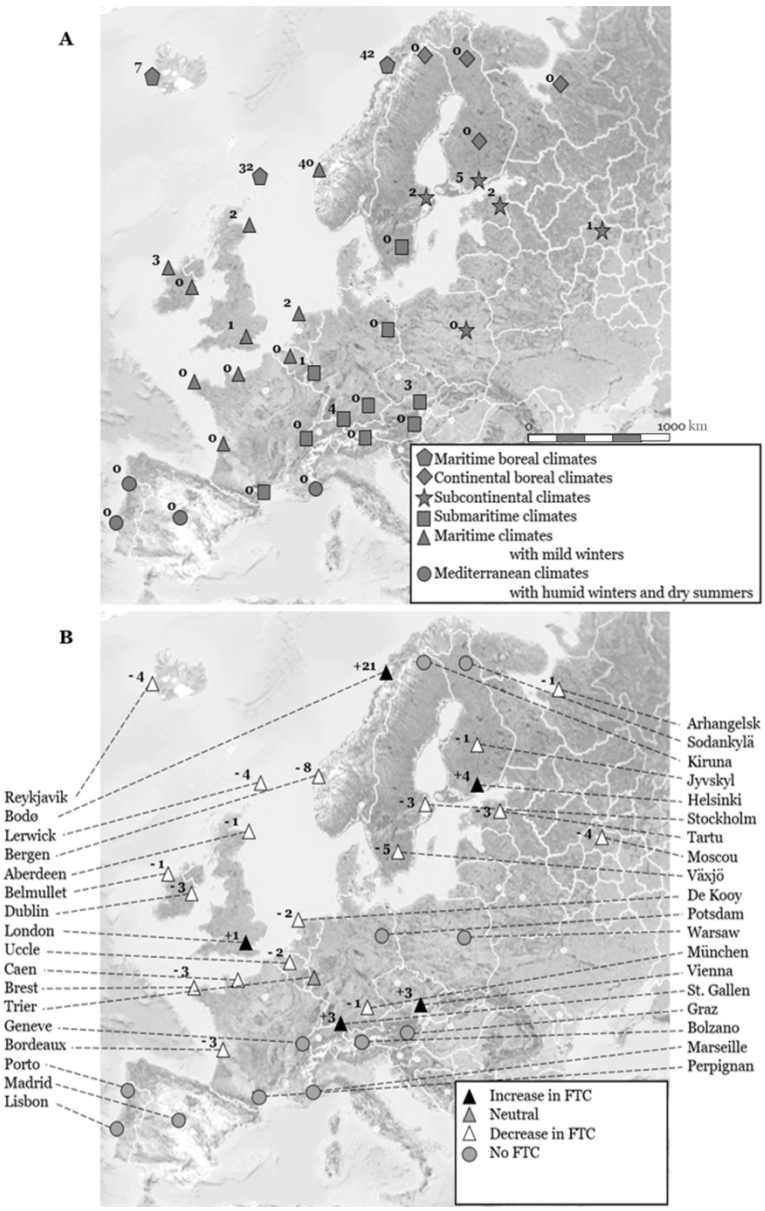


Figure 4 The number of critical freeze-thaw-cycles (FTC) for TMY 2000-2009 (A) and increase in number of critical FTC between TMY 1961-1990 and TMY 2000-2009 (B) across Europe (map: Google Earth, 2018)

119x184mm (300 x 300 DPI)

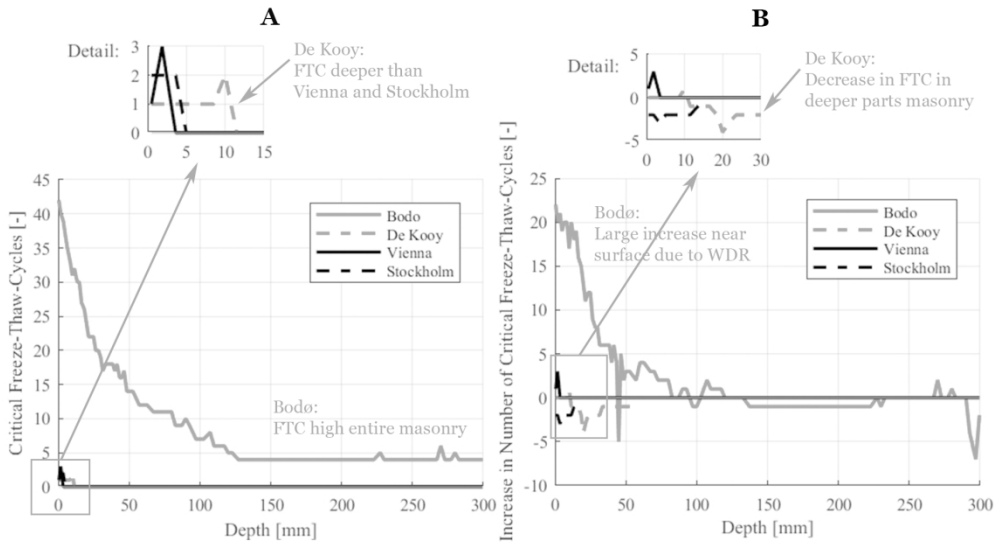


Figure 5 The number of critical freeze-thaw-cycles (FTC) for TMY 2000-2009 (A) and increase in number of critical FTC between TMY 1961-1990 and TMY 2000-2009 (B) in Bodø , De Kooy, Vienna and Stockholm

160x88mm (300 x 300 DPI)